Erschienen in: The European Physical Journal Special Topics ; 222 (2013), 11. - S. 2819-2833
https://dx.doi.org/10.1140/epjst/e2013-02060-5

Force-driven micro-rheology

Th. Voigtmann[1,2,3] and M. Fuchs[1]

[1] Fachbereich Physik, Universität Konstanz, 78457 Konstanz, Germany
[2] Zukunftskolleg, Universität Konstanz, 78457 Konstanz, Germany
[3] Institut für Materialphysik im Weltraum, Deutsches Zentrum für Luft- und Raumfahrt (DLR), 51170 Köln, Germany

Abstract. Within a microscopic formalism for the nonequilibrium response of colloidal suspensions driven by an external force, we study the active micro-rheology of a glass-forming colloidal suspensions. In this technique, a probe particle is subject to an external force, and its nonequilibrium dynamics is monitored. Strong external forcing delocalizes the particle from its nearest-neighbor cage, resulting in a pronounced force-thinning behavior of the single-particle friction. We discuss the dynamics in the vicinity of this delocalization transition, and how long-range transport is induced for a particle that is localized in the quiescent case.

1 Introduction

Colloidal dispersions offer unique possibilities to obtain mesoscopic information on the dynamics of soft matter under large applied fields. One promising technique is active force-driven microrheology, where a single probe particle is driven by an external force through the embedding host medium [1–4]. This can be achieved through laser tweezers or magnetic forces, or even through chemical reactions on (anisotropically) surface-treated particles [5]. The probe is typically comparable in size to those comprising the host system, which makes active microrheology an ideal tool suited to probe the dynamics of complex fluids [6–9], granular matter [10–13] and, e.g., cellular matter on the mesoscopic scale of its constituents [14–17]. Yet this implies that a coarse-grained description where one treats the latter as a continuum is not applicable.

In dense environments, the motion of the forced probe particle is governed by slow structural relaxation of the surrounding host system [18–20]. This induces striking nonlinearities in the force–velocity relations measured for the pulled probe particle. In particular, if the host density is high enough so that it is close to a glass transition where kinetic arrest occurs, the relaxation time of host-particle density fluctuations becomes arbitrarily large. This implies that even small forces (on the order of pN or less in soft matter) are sufficient to leave the linear response regime. One then needs to understand the nonlinear friction induced by the slow structural relaxation.

Theoretical understanding of active microrheology is often based on the low-density regime [21–23]. Here, the equations of motion can be solved exactly in the

leading order in density, viz. the two-particle Smoluchowski equation for colloidal suspensions. In this approach, hydrodynamic interactions that are mediated by the solvent between the particles, are important. One finds that the correlations among particles exhibit two different spatial regions: In the far field, the external forcing effectively overwhelms thermal fluctuations and randomizes the system. Close to particle contact, however, Brownian motion and external forcing compete and cause the build-up of a boundary-layer, especially for large Peclet numbers. It determines the friction and the force-velocity relation of the probe. The Peclet number measures the force induced velocity in relation to the intrinsic diffusion and indicates when the force-velocity relation becomes non-linear. For anisotropic particles, insights can already be gained by considering the trajectories of individual e.g. Brownian ellipsoids [24,25]. Their effective friction is determined by the Lagrangian unsteadiness experienced by the solvent flow, and the spatially inhomogeneous and rheologically mixed strain field set up around the probe. The low-density theory of microrheology has the advantage of being exact, but it is not easily extended to higher densities, since a perturbative approach to the collective dynamics close to the glass transition is not adequate. Ad-hoc models of glass relaxation have been extended to deal with active microrheology [26], but there, the collective aspects of the probe-to-host particle coupling are not treated. Simulations have revealed that the depinning of the probe in a dense environment is accompanied by anomalous fluctuations which reveal the spatial and dynamical heterogeneities in glass-forming systems [27,28]. These phenomena will be the focus of the present mini-review.

We consider in the following the case of a single probe particle driven by a strong external force through a glass-forming colloidal suspension. Other modes of driving are possible, such as constant-velocity microrheology [29–31] or particles pulled along a harmonic-potential trap [32,33]. The many-particle Smoluchowski equation is not amenable to exact treatment. Yet, for the slow structural relaxation especially in colloidal glass formers, the mode-coupling theory of the glass transition (MCT) [34] offers a microscopic description that is able to capture the main aspects of the ensuing dynamics quantitatively. This MCT has been extended to include nonequilibrium driving, based on an integration-through-transients (ITT) approach of nonequilibrium statistical physics [35,36]. This was first done for bulk shear flow [37,38]. In a similar spirit, the ITT-MCT was formulated for active force-driven microrheology [39,40]. One arrives at a first-principles description of the dynamics of a pulled tracer in a glass-forming host suspension. Here, hydrodynamic interactions are neglected, which is an approximation suitable for high densities and presumably not too large forces.

Solving the ITT-MCT equations numerically, one obtains predictions for the force–velocity relations, but also the statistics of the probe dynamics [41], based only on the equilibrium static structure information. This route is technically very demanding, since one has to deal with integral equations of motion covering exponentially large timescales, spatial anisotropies, and possible instabilities in the discretized version of the equations [42].

To give a qualitative account of measured data, one thus introduces ad-hoc simplifications of the full ITT-MCT. These “schematic models” have been very fruitful in understanding the liquid–glass transition in the quiescent state [34], but also for the bulk-shear version of ITT-MCT [43]. Here they already contain the essence of the kinetic arrest transition and its modification through external driving. They are guided by the ITT-MCT result that fluctuations on spatial length scales around the interparticle separation dominate the dynamics. Schematic models for active microrheology have to account for spatial anisotropy, but otherwise ignore length scales. Nevertheless they are successful in describing force–velocity relations [44], or the stochastic dynamics of the tracer around its mean path [45]. They have also been used to derive asymptotic scaling laws for the friction coefficient [46].

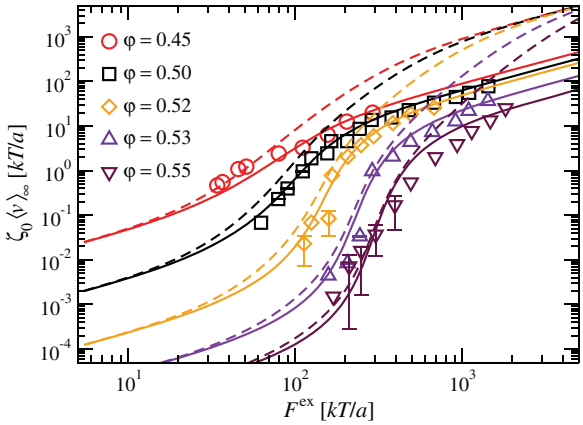

Fig. 1. Probe-particle steady-state velocity $\langle v \rangle_\infty$ as a function of the applied external force F^{ex}. Quantities are expressed in thermal-force units, kT/a, where a is the average radius of a bath particle. ζ_0 is the bare friction coefficient of a single tracer particle. Figure adapted from Ref. [44].

In this paper, we review recent results obtained by the ITT-MCT and schematic MCT (sMCT) descriptions of nonlinear, force-driven active microrheology in glass-forming colloidal suspensions. An introduction to typical experimental results is given in Sect. 2, after which the novel features of the theory are discussed in Sect. 3. We then proceed to discuss the characteristics of localized probes (Sect. 4) and the dynamics of the pulled probe particle in more detail (Sect. 5).

2 Force-velocity relations

Figure 1 shows typical force-velocity relations obtained in dense host suspensions. Data is shown from the experiment by Habdas et al. [19]; there, a magnetic bead with size $a^s \approx 2.5a$ relative to the bath-particle size a was pulled with various constant forces, and the bath density was varied, approaching the glass transition from the liquid side. At the lowest forces accessible in that experiment, the velocity–versus–force curves increase superlinearly, before bending over to a regime of linear variation at the highest forces shown. The superlinear regime becomes more pronounced with increasing bath-particle density, and occurs in a range of $F^{\mathrm{ex}} = \mathcal{O}(100\,kT/a)$, i.e., on a scale much larger than expected from forces induced by thermal fluctuations.

At lower forces than probed in experiment, one expects a linear-response regime where $v \propto F^{\mathrm{ex}}$, defining a force-independent friction coefficient ζ as the coefficient of proportionality. This is indeed indicated for the lowest-density experiment shown, and was verified in Ref. [19] for a pulled particle in a dilute host suspension. Upon increasing density, the linear-response mobility of the tracer decreases dramatically as a precursor of the glass transition. Hence, the linear-response regime can no longer be resolved in experiment. Recall that for a colloidal particle of radius a, a typical linear-response velocity scale is $v \sim (kT/a)/\zeta_0$. Using $kT \approx 4\,\mathrm{pN\,nm}$ and the Stokes expression for the friction coefficient, $\zeta_0 = 6\pi\eta a$ with the solvent viscosity $\eta \approx 1\,\mathrm{mPa\,s}$, this translates to $v \sim 0.2/a^2\,\mu\mathrm{m}^3/\mathrm{s}$. For the experiment shown in Fig. 1, particles are roughly $a = 1\,\mu\mathrm{m}$ in size, hence the velocity scale is $0.2\,\mu\mathrm{m/s}$. As the density is increased to the vicinity of the glass transition, the increase in the linear-response friction causes v to drop by about four orders of magnitude. A linear-response

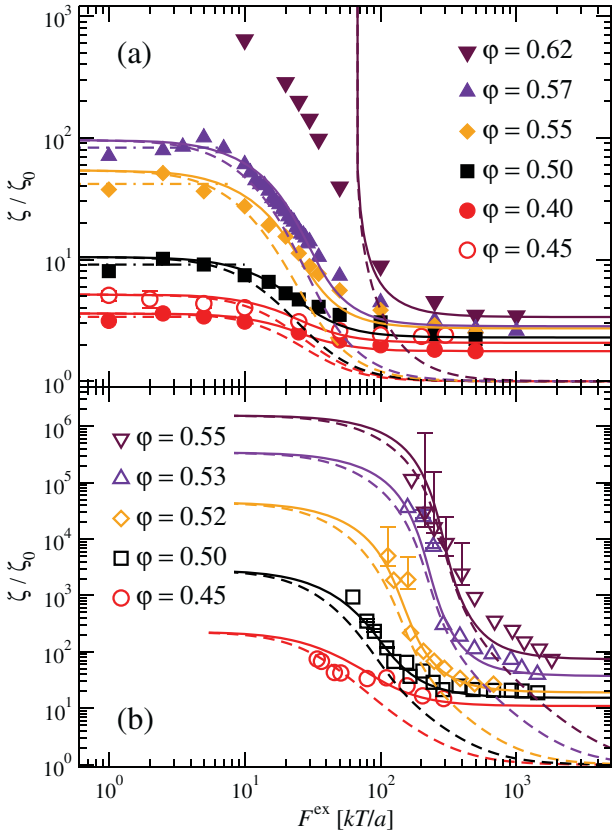

Fig. 2. Nonlinear friction coefficient $\zeta(F^{\rm ex})$ of a forced probe particle in dense colloidal suspensions, as a function of the applied force, normalized by the free-particle solvent friction ζ_0. (a) Results from stochastic-dynamics simulations of polydisperse quasi-hard-spheres (filled symbols) at packing fractions φ as labeled. Open symbols are Brownian-dynamics simulation results for monodisperse hard spheres from Ref. [47]. (b) Symbols are experimental results translated from Fig. 1. Solid lines in both panels are fits using a schematic model of mode coupling theory as outlined in the text. Dashed lines are fits using the same model, but neglecting a friction contribution from density fluctuations with Fourier components perpendicular to the applied force. From Ref. [44].

measurement at this density would require to resolve particle motion over μm in weeks. (This is a similar problem for NEMD simulations, albeit less severe.)

Mode-coupling theory rationalizes the superlinear increase of $v(F^{\rm ex})$ as the signature of a force-induced depinning transition. This is best discussed in terms of the single-particle friction coefficient $\zeta(F^{\rm ex})$, defined through

$$\zeta(F^{\rm ex})\,\langle \mathbf{v}\rangle_{t\to\infty} = \mathbf{F}^{\rm ex}\,, \tag{1}$$

where $\langle \mathbf{v}\rangle_{t\to\infty}$ is the stationary velocity average. The superlinear increase in the velocity observed in Fig. 1 corresponds to a strong decrease in the friction coefficient as a function of applied force. This is shown in Fig. 2, where the data of Fig. 1 have been transformed, and also computer-simulation results [39,44] are shown.

For the computer simulation, the approach to linear response is clearly seen at the lower densities. At the highest density, $\varphi = 0.62$, the undriven system is not able to equilibrate on the time scale of the simulation runs. Correspondingly, a

linear-response friction coefficient could not be defined, and the points corresponding to the lowest four forces in Fig. 2 would still be subject to a slight increase if the simulation were run longer, due to aging effects in the glass.

The lines shown in Figs. 1 and 2 are fits with a schematic model of mode-coupling theory, outlined below. The solid line fitted to the $\varphi = 0.62$ simulation data in Fig. 2a demonstrates the depinning transition predicted to occur in the ideal glass. At zero force, the probe-particle mobility is zero in the glass. This holds except for special cases like very small probe particles whose equilibrium dynamics already decouples from the host liquid [48]. We will not discuss the latter scenario in the present context. Very small forces are not expected to induce a finite mobility for the probe particle on the time scale of stability of the glassy host, since the host solid is able to sustain a certain amount of (local) stress. This is particularly true for ideal hard-sphere glasses, where MCT predicts infinite barriers for a single particle to escape its nearest-neighbor cage.

If the external force exceeds a certain (density-dependent) threshold, the probe particle is forced free out of its nearest-neighbor cage, and a finite mobility indicating long-range motion results. In the liquid close to the glass transition, nearest-neighbor cages are still present, albeit not persistent. Hence, the signature of the depinning transition remains visible as a strong decrease of the friction coefficient with increasing force. This explains naturally the strong forces required to enter the force-thinning regime, or equivalently, the superlinear increase in the probe-particle velocity: the threshold force is determined not by thermal fluctuations, but by the local rigidity of the embedding solid (persistent or not). It is thus a measure of a typical cage strength. Loosely one can use the force threshold to estimate the degree of cooperativity in the cage formation. Attributing $1kT/a$ to each thermally excited degree of freedom of particles with radius a, of the order of some tens to (a few) hundred particles appear to contribute to the cage strength. Not surprisingly, the force-velocity curves entering the glassy regime indicate that the cage strength, viz. number of cooperative particles, increases with packing fraction.

3 Mode-coupling theory

The mode-coupling theory for active microrheology starts from an integration-through-transients (ITT) formalism that allows to derive generalized Green-Kubo relations connecting transport coefficients and so-called transient correlation functions in the nonlinear-response regime.

One starts from the Smoluchowski equation describing the motion of N host-system particles and a single tracer. The nonequilibrium distribution function $\psi(\Gamma, t)$ obeys $\partial_t \psi(\Gamma, t) = \Omega(\Gamma)\, \psi(\Gamma, t)$, where $\Gamma = \{\mathbf{r}_1, \ldots \mathbf{r}_N, \mathbf{r}_s\}$ is the configuration-space element spanned by the particle positions. We assume that the particles are spherical and do not possess internal degrees of freedom that couple to the dynamics. The Smoluchowski operator $\Omega(\Gamma)$ is then given as

$$\Omega = \sum_{i=1,\ldots N,s} \partial_i \cdot (kT\partial_i - \mathbf{F}_i)/\zeta_i - (\partial_s \cdot \mathbf{F}^{\mathrm{ex}})/\zeta_s \,, \tag{2}$$

where the last term $\delta\Omega = -(\partial_s \cdot \mathbf{F}^{\mathrm{ex}})/\zeta_s$ is the nonequilibrium driving term. Here, ζ_i and ζ_s are the Stokes friction coefficients for individual host and probe particles. For simplicity, we neglect hydrodynamic interactions among the particles.

The integration-through-transients (ITT) formalism starts by deriving an operator identity expressing the time-dependent nonequilibrium distribution function as a history integral where the equilibrium distribution $\psi_{\mathrm{eq}} \propto \exp[-\beta U]$ appears

(where U is the potential energy of the system). For Eq. (2), we get, recalling $\Omega\psi_{\rm eq} = \delta\Omega\psi_{\rm eq} = -(\mathbf{F}_s \cdot \mathbf{F}^{\rm ex})/(kT\zeta_s)\psi_{\rm eq}$,

$$\psi(t) = \psi_{\rm eq} - \frac{1}{kT\zeta_s}\int_0^t dt' \exp[\Omega t'](\mathbf{F}^{\rm ex} \cdot \mathbf{F}_s)\psi_{\rm eq}\,, \tag{3}$$

assuming that the external force was switched on instantaneously at $t = 0$, starting from an equilibrium configuration. The friction coefficient is obtained by using this equation to average the fluctuating probe velocity $\mathbf{v}_s = (\mathbf{F}_s + \mathbf{F}^{\rm ex})/\zeta_s$. Here, a standard problem recognized in the theory of dense colloidal suspensions arises [49,50]: the resulting expression is not guaranteed to be positive if approximations are later introduced, since it subtracts from the free-drag velocity the interaction contributions. To arrive at a better-suited starting point for mode-coupling approximations, one rewrites this in terms of the irreducible dynamics. Following a Dyson decomposition of the time-evolution operator, one obtains [40]

$$\zeta = \zeta_s + \frac{1}{3kT}\int_0^\infty dt\, \langle \mathbf{F}_s \exp[\Omega^{\rm irr}(\mathbf{F}^{\rm ex})t]\mathbf{F}_s\rangle_{\rm eq}\,, \tag{4}$$

where the exact form of the irreducible Smoluchowski operator $\Omega^{\rm irr}$ is not relevant in the present context. It is an important result of the ITT formalism that this latter average is taken with the *equilibrium* distribution function (assumed to be well known), but contains the full nonequilibrium time evolution. Equation (4) has the familiar form of a Green-Kubo relation, extended to the nonlinear response regime because the correlation function appearing under the integral contains the nonlinear perturbation in its time evolution. The relation recovers the classical Green-Kubo law if the latter dependence is neglected. The correlation function is called transient since it is formed with the equlibrium average [36].

The mode-coupling approximation to Eq. (4) is based on the assumption that the slow decay of host-particle and probe-particle density fluctuations is the dominant contribution to the friction coefficient. Projecting the dynamics in Eq. (4) to the simplest nontrivial combination, the product of a host- and a probe-particle density, one obtains an integral over a specific four-point correlation function. The latter is, as part of the mode-coupling approximation split into a product of two-point density correlation functions, at the same time replacing their irreducible time evolution with the full one. One then arrives at

$$\langle \mathbf{F}_s \exp[\Omega^{\rm irr}t]\mathbf{F}_s\rangle \approx \sum_{\mathbf{k}} \frac{|kTkS_k^s|^2}{NS_k}\phi_{\mathbf{k}}^s(t)\phi_{-\mathbf{k}}(t)\,, \tag{5}$$

where $\phi_{\mathbf{k}}(t) = \phi_k(t) = \langle \varrho_{\mathbf{k}} \exp[\Omega^\dagger t]\varrho_{\mathbf{k}}\rangle_{\rm eq}$ is the collective transient density correlation function of the host particles, and $\phi_{\mathbf{k}}^s(t) = \langle \varrho_{\mathbf{k}}^s \exp[\Omega^\dagger t]\varrho_{\mathbf{k}}^s\rangle_{\rm eq}$ is the transient probe-particle density correlator. Here, $\varrho_{\mathbf{k}} = \sum_{j=1}^N \exp[i\mathbf{k}\cdot\mathbf{r}_j]$ and $\varrho_{\mathbf{k}}^s = \exp[i\mathbf{k}\cdot\mathbf{r}_s]$ are the collective host-particle, and probe-particle density fluctuations, respectively. It should be noted that we assume spatial isotropy and translational invariance to hold in the thermodynamic limit, since the single probe particle will have negligible influence on the statistical properties of the system. Under this assumption, the host-particle correlator $\phi_k^s(t)$ does not depend on the direction of the wave vector $\mathbf{k}$.

For the density correlators, mode-coupling equations of motion are derived following the standard procedure for colloidal suspensions [51]. Since the nonequilibrium term in Eq. (2) acts only on the probe-particle degrees of freedom, the equation of motion for $\phi_k(t)$ is exactly as in equilibrium, discussed in depth in connection with

the glass transition [34]. For the probe-particle correlator, a similar equation holds,

$$\omega_{\mathbf{q},\mathbf{q}}^{-1}\partial_t\phi_{\mathbf{q}}^s(t)+\phi_{\mathbf{q}}^s(t)+\int_0^t m_{\mathbf{q}}^s(t-t')\partial_{t'}\phi_{\mathbf{q}}^s(t')\,dt'=0\,. \tag{6}$$

Here, $\omega_{\mathbf{q},\mathbf{p}}=(\mathbf{q}-\mathbf{i}\mathbf{F}^{\mathrm{ex}})\cdot\mathbf{p}/\zeta_{\mathbf{s}}$. The effect of the slow structural-relaxation dynamics of the host enters through the memory kernel,

$$m_{\mathbf{q}}^s(t)=\int\frac{d^3k}{48\pi^2\varphi}\frac{S^s(p)^2}{S(p)}\frac{(\mathbf{q}\cdot\mathbf{p})\omega_{\mathbf{q},\mathbf{p}}}{\omega_{\mathbf{q},\mathbf{q}}^2}\phi_p(t)\phi_{\mathbf{k}}^s(t)\,. \tag{7}$$

Here, $\varphi=(\pi/6)\varrho$ is the packing fraction of the host system, taken to be at number density ϱ and choosing the particle diameter as the unit of length. $S(p)$ and $S^s(p)$ are the static structure factors characterizing the equilibrium structure and interactions of the host particles and the embedded probe. These are taken from standard liquid-state theory; for a system of hard spheres the Percus-Yevick approximation [52] is employed to arrive at a parameter-free prediction of the dynamics.

Equation (6) encodes a number of symmetries that are preserved by the mode-coupling approximation to the memory kernel. First one notices that $\phi_{\mathbf{k}}^s(t)$ is in general complex-valued, since it is an auto-correlation function formed with a non-Hermitian operator. There holds $\phi_{\mathbf{k}}^s(t)^*=\phi_{-\mathbf{k}}^s(t)$. Under rotational symmetry around the force axis, this implies that $\phi_{\mathbf{k}}^s(t)$ remains real-valued for all $\mathbf{k}\perp\mathbf{F}^{\mathrm{ex}}$.

The ideal glass is signalled by a non-decaying contribution to the density-correlation functions, called the nonergodicity parameter or glass form factor $f_q=\lim_{t\to\infty}\phi_q(t)$. In the ordinary case where also the unforced probe-particle motion arrests in the glass, we have $f_{\mathbf{q}}^s=\lim_{t\to\infty}\phi_{\mathbf{q}}^s(t)>0$ at the same time. An explicit equation for this probe-particle nonergodicity parameter can be obtained from Eq. (6), as

$$f_{\mathbf{q}}^s=\frac{m_{\mathbf{q}}^s[f,f^s]}{1+m_{\mathbf{q}}^s[f,f^s]}, \tag{8}$$

where it is understood that $m_{\mathbf{q}}^s$ is evaluated from Eq. (7) with $\phi_p(t)$ and $\phi_{\mathbf{k}}^s(t)$ replaced by f_p and $f_{\mathbf{k}}^s$, respectively.

Using rotational symmetry around the axis of the applied force, one can solve the ITT-MCT equations of motion on a discrete grid of wave-vector magnitudes and angles between $\mathbf{q}$ and $\mathbf{F}^{\mathrm{ex}}$. For details on the numerical scheme we refer to Ref. [42]. The solution of the full ITT-MCT equations is still a numerically very demanding task.

To ease the discussion of the effects induced by the long-lasting memory kernel in Eq. (6), a schematic model has been devised that reduces the spatial dependence of all wave-vector dependent quantities to one only on the alignment with respect to the external force. The model is defined by two probe-particle correlation functions $\phi_\perp^s(t)$ and $\phi_\parallel^s(t)$, together with a single host-particle correlator $\phi(t)$, setting

$$(1/\omega_\alpha)\partial_t\phi_\alpha^s(t)+\phi_\alpha^s(t)+\int_0^t m_\alpha^s(t-t')\partial_{t'}\phi_\alpha^s(t')\,dt'=0, \tag{9}$$

$$(1/\Gamma)\partial_t\phi(t)+\phi(t)+\int_0^t m(t-t')\partial_{t'}\phi(t')\,dt'=0, \tag{10}$$

with $\alpha\in\{\perp,\parallel\}$ and $\omega_\parallel=\omega_\perp(1-i\kappa_\parallel F^{\mathrm{ex}})$. The parameters Γ and $\omega_\perp$ set the unit of time and define the bare friction coefficient for the probe particle, while $\kappa_\parallel$ serves to

set the unit of forces. All these parameters are used in fitting data, but are inessential for the qualitative behavior of the model. The memory kernels of the schematic model are defined as

$$m^s_\parallel(t) = \left[v^s_1\phi^{s*}_\parallel(t) + v^s_2\phi^s_\perp(t)\right]\phi(t)/(1 - i\kappa_\parallel F^{\rm ex}), \tag{11}$$

$$m^s_\perp(t) = \left[v^s_1\phi^s_\perp(t) + v^s_2\Re\phi^s_\parallel(t)\right]\phi(t)/[1 + (\kappa_\perp F^{\rm ex})^2], \tag{12}$$

$$m(t) = v_1\phi(t) + v_2\phi(t)^2. \tag{13}$$

The latter is the well-known F_{12} model of glassy dynamics [34], allowing to capture schematically the approach of the host liquid to a glass transition. Its coupling coefficients v_1 and v_2 determine the state of the host, and the model exhibits a line of critical glass-transitions points (v^c_1, v^c_2). The coefficients $v^s_{1,2}$ adjust the strength of the probe–host particle interaction, and mimic the wave-vector dependent vertices appearing in Eq. (7). The specific choice of complex conjugated and real parts of $\phi^s_\alpha(t)$ in the memory kernels captures the symmetry properties of the full ITT-MCT.

The schematic-MCT (sMCT) model is complemented by a Green-Kubo-like expression for the friction coefficient, $\zeta(F^{\rm ex}) = 1 + \Delta\zeta(F^{\rm ex})$,

$$\Delta\zeta(F^{\rm ex}) = \mu\int_0^\infty \phi(t)\phi^s_\perp(t)\,dt + (1-\mu)\int_0^\infty \phi(t)\Re\phi^s_\parallel(t)\,dt, \tag{14}$$

which again is dictated by symmetry considerations. Here, the mixing parameter μ has to be introduced to allow adjusting the relative weight of friction contributions from the two chosen spatial directions. Based on low-density theory where the ratio of $\Delta\zeta(0)/\Delta\zeta(\infty) = 2$ [53] one would expect $\mu = 1/2$. Note however, that in the high-density regime, this fixed ratio is not observed, as is evident from Fig. 2.

4 Density distributions of pinned probes

A specific prediction of ITT-MCT is the existence of a critical force $F^{\rm ex}_c$ in the glass, where the probe particle motion decouples from that of the host system. This corresponds to a regime where $f^s_{\mathbf{q}} \equiv 0$, even though $f_q \neq 0$.

In the localized regime, $f^s_{\mathbf{q}} \neq 0$ holds, and one can identify the Fourier back-transform of the probe-particle glass-form factor with the probability distribution indicating the position of the probe,

$$f^s(\mathbf{r}) = \int \frac{d^3q}{(2\pi)^3} f^s_{\mathbf{q}}\,. \tag{15}$$

By construction, this quantity is zero both in the delocalized regime and in the liquid, since in the ensemble average the probe is equidistributed over all space. (This already implies that there is force-induced diffusion even in directions perpendicular to the driving; an issue that we will discuss below.) In the case of a localized probe in the glass, $f^s(\mathbf{r})$ can be measured in simulation by evaluating the van Hove correlation function of the probe particle at a sufficiently large time, chosen still small enough so that the eventual decay of density correlations observed in the non-ideal glass does not interfere. In principle, this allows to estimate $f^s(\mathbf{r})$ even in equilibrated simulations in the liquid, if the state is close to the glass transition.

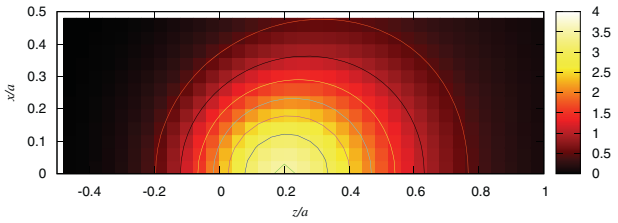

Fig. 3. Density plot of a 2-dimensional cut of the probe-particle distribution function $f^s(\mathbf{r})$, evaluated from ITT-MCT at the glass-transition point for a hard-sphere system with a probe of equal size, at $F = 10\,kT/a$ (directed to the right along the abscissa). From Ref. [41]. Reprinted with permission from De Gruyter.

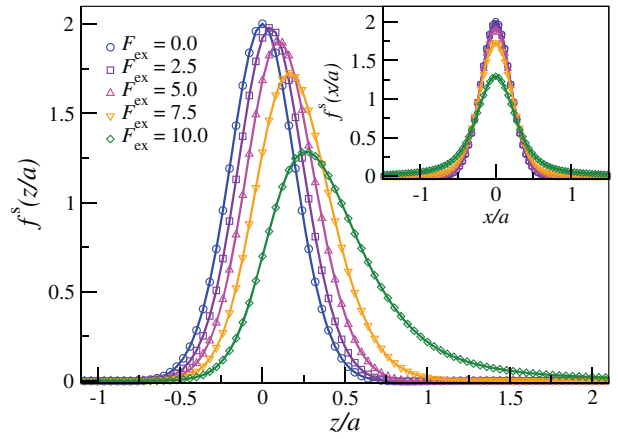

Fig. 4. Marginal probability density for the probe-particle location along the force axis, for various external forces at the MCT glass transition in the hard-sphere system. The inset shows the corresponding marginal probability distributions along an axis perpendicular to the force. From Ref. [41]. Reprinted with permission from De Gruyter.

Figure 3 shows a contour plot of $f^s(\mathbf{r})$ obtained from the microscopic ITT-MCT calculation. A two-dimensional cut through a plane containing the force-direction is shown; the full distribution is rotationally invariant around this latter axis. A state at the MCT glass transition was chosen, with an external force still sufficiently below the delocalization threshold.

One clearly notices two features: the center of the distribution is shifted from zero in the direction of the applied force. The second feature is a distortion of the distribution in the direction of the force. The probability falls off less quickly along the positive force axis than it does in the opposite direction.

To quantify this, is is convenient to discuss one-dimensional marginal probability densities obtained by integrating all but one spatial direction. Figure 4 shows exemplary results close to the glass transition, for the distribution along the force axis, $f^s(z)$, and (in the inset) for the distribution along the axis perpendicular to that, $f^s(x)$. Several forces below the delocalization threshold are shown. As dictated by symmetry, the distribution orthogonal to the force remains centered on zero, while the peak of the in-force-directed distribution shifts as anticipated from Fig. 3. For the largest force shown it is apparent that the distribution also develops a heavy tail in the force direction. As a result, it becomes positively skewed. Interestingly, also the orthogonal distribution $f^s(x)$ shows indications of heavy tails in both directions for the largest force. Indeed one can decompose the distribution into a roughly Gaussian

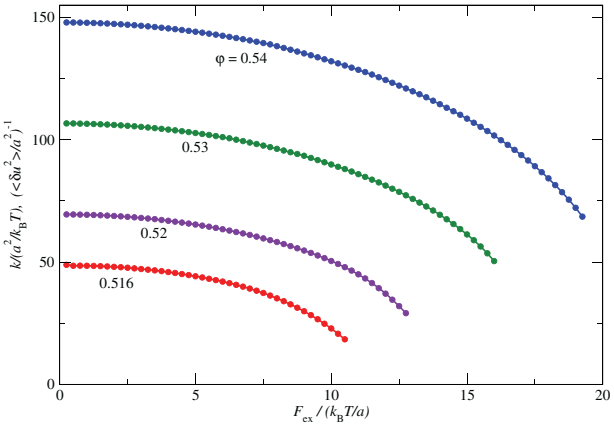

Fig. 5. Effective spring constant k obtained from the finite long-time displacement of a localized probe in the ideal glass, for various host-system packing fractions φ as indicated. Symbols are calculated using ITT-MCT for hard spheres. Figure adapted from Ref. [41].

center, and exponential tails [42]. The latter correspond to increasingly long-ranged rare excursions of the probe particle even in its localized state, as a precursor to complete delocalization. The schematic model and earlier analysis of the data emphasized only this long-range contribution to the delocalization, neglecting the tightly localized center of the distribution. In a simple schematic model, such a distinction is not built in, since the model lacks the proper spatial resolution.

From the force-dependent displacement of the probe particle in the localized regime, one can estimate an effective spring constant $k = F^{\mathrm{ex}}/\langle \delta z \rangle$, where δz denotes the finite long-time asymptote of the probe displacement, relative to its starting position. Figure 5 shows results based on ITT-MCT for hard-sphere glasses of various density. As $F^{\mathrm{ex}} \to 0$, the linear-response cage rigidity can be read off from this graph. The values are in good agreement with those reported from a computer simulation [54]. At larger forces, force-induced softening sets in, i.e., the spring constant k decreases with increasing F^{ex}. Following linear-response theory, the low-force spring constants can also be connected to the fluctuations of the probe displacement [41]. In this regime, the response is still close to isotropic, but as anticipated from Fig. 3 already for moderate forces, noticable spatial anisotropies set in and cause deviations from the linear-response behavior.

5 Dynamics

For the following discussion of dynamical properties, we restrict ourselves to the schematic MCT (sMCT). First a priori calculations for the dynamics within full ITT-MCT can be found in Ref. [42].

A central quantity for MCT are the transient density correlation functions. A comparison of the sMCT results with computer simulation is shown in Fig. 6. Due to the force-induced anisotropy, density fluctuations with wave vectors aligned with the external force and those perpendicular to it play a qualitatively different role. If the probe particle moves along the force, a phase modulation of the corresponding density correlation function results. Hence, this correlation function becomes complex-valued and shows strong oscillations with a frequency that can be related to the drift velocity at high forces [46]. As seen in Fig. 6, this qualitative behavior is well captured by the schematic MCT. In the direction perpendicular to the force, there is no systematic

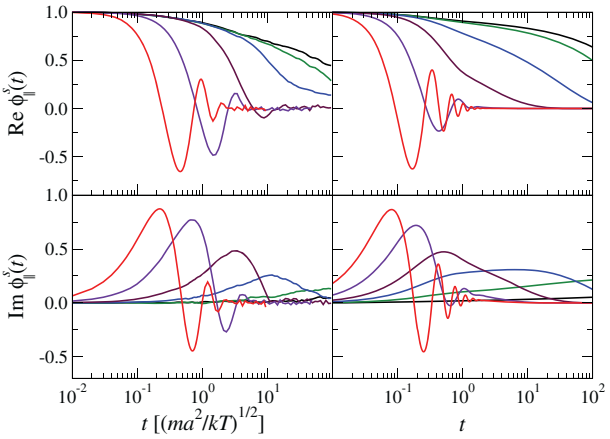

Fig. 6. Density correlation function from a schematic-MCT model of active microrheology (right), compared with results from a stochastic-dynamics simulation (left, evaluated at wave vectors corresponding to the first maximum in the static structure factor). Correlators are shown for fluctuations in the direction of the force, displaying both real and imaginary parts. Figure from Ref. [44].

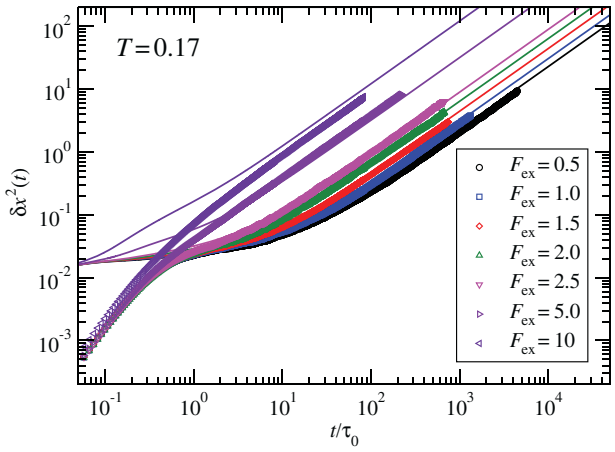

Fig. 7. Mean-squared displacements of the probe particle measured in the direction orthogonal to the applied force, for a MD simulation of a glass-forming binary Yukawa mixture (symbols), at a fixed temperature in the liquid close to the glass transition, for increasing applied force. Lines are fits using schematic MCT. From Ref. [45].

drift for the probe particle. The corresponding symmetry demands that the correlation function remains real-valued, as is indeed verified by computer simulation [44].

It is already implicit in the above discussion, that for the delocalized particle, long-range motion also perpendicular to the force sets in. This is a consequence of the mode-coupling integral which introduces a coupling between density fluctuations in all spatial directions. Consequently, the delocalization transition marks the point where a finite $f^s(\mathbf{r})$ becomes zero everywhere.

The force-induced diffusion has been studied in detail in Ref. [45], employing the schematic-MCT model, and fitting to computer simulations [27,28]. The result for the mean-squared displacement in the direction orthogonal to the applied force is shown in Fig. 7. Apart from a qualitative difference at short times that arises because the

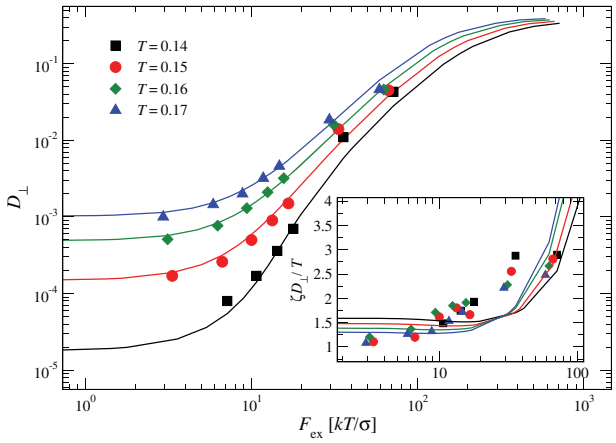

Fig. 8. Force dependence of the probe-particle diffusion coefficient orthogonal to the applied force, for a binary Yukawa mixture (symbols from MD simulations) and a schematic-MCT fit (lines); various temperatures close to the glass transition as labeled. The inset shows the Stokes-Einstein ratio $\zeta D/T$. From Ref. [45].

simulations use thermostatted Newtonian equations of motion, while the theory works with the overdamped Brownian dynamics, the schematic model qualitatively explains the simulation data. As the force is increased, the diffusivity of the probe particle is increased by orders of magnitude. Here it should be noted that the simulations were carried out in a liquid host, where already for zero external force, a finite long-time diffusivity of the probe remains.

Since the orthogonal MSD become diffusive for long times even in the presence of the external force, it is possible to extract force-dependent diffussion coefficients. These are shown in Fig. 8 for a set of different simulational temperatures. Qualitatively, the shape of the D-versus-F^{ex} curves resembles that of the inverted friction-coefficient graphs. However, the "Stokes-Einstein-Sutherland" product $\zeta D/T$ is roughly constant only for the smallest forces, as shown in the inset of Fig. 8. Once the external force becomes comparable to the delocalization threshold, the motion in the direction of the force (quantified by ζ) decouples from the diffusive motion perpendicular to it (quantified by D). Indeed, the motion along the force axis becomes much more efficient, as seen from the fact the $\zeta D/T$ grows with increasing force. In MD simulations [27,28] it was indeed found that the statistics of the motion around the mean path in the direction of the force becomes superdiffusive.

Let us mention a few features of the dynamics at very large forces. It is an intriguing finding obvious from Fig. 2 that in this regime, the probe-particle friction coefficient does not approach that of the bare solvent as expected for a free particle. This is even true at low densities, where it arises from a hydrodynamic boundary-layer phenomenon [21]. In this regime, one finds in particular a fixed ratio between the low-force linear-response friction coefficient $\zeta(0)$ and the one at infinite force $\zeta(\infty)$: $\zeta(0)/\zeta(\infty) = 2$, as found in a rigorous treatment of the Smoluchowski equation on the two-particle level, and verified in simulations [22].

At high densities, the fixed ratio $\zeta(0)/\zeta(\infty)$ is no longer found, reflecting the fact that $\zeta(0)$ is governed by collective particle interactions, while $\zeta(\infty)$ arises from features of the short-time two-body dynamics.

The high-force plateau in the friction coefficient increases much less than $\zeta(0)$ when increasing the density. According to the low-density theory, it scales with the contact value of the radial distribution function. This is tested in Fig. 9, where we

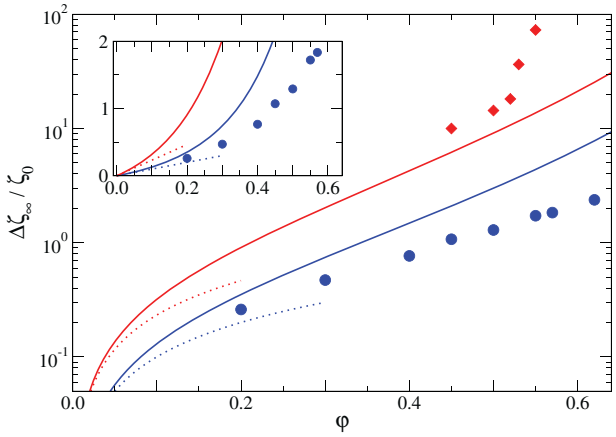

Fig. 9. $\Delta\zeta(F^{\rm ex} \to \infty)$ as a function of packing fracion. From Ref. [44].

plot the values obtained from computer simulation and also from experiment. Lines are the theoretical predictions, using a correction of the low-density contact value according to an empirical equation of state [44]. It is found that the increase of $\zeta(\infty)$ with increasing density iNonlinear friction coefficients qualitatively captured by the corresponding increase in contact values, confirming that this part of the friction-versus-force curves is governed by the physics of two-particle collisions.

In the schematic MCT model, a finite increment over the solvent friction remains even for $F^{\rm ex} \to \infty$ if one assumes density fluctuations to wave vectors perpendicular to the force to contribute significantly in the Green-Kubo integral. For the full MCT, this question is still open.

Interestingly, recent simulations on a driven particle in a granular system [13] do not show a large-force plateau in the friction coefficient. Instead, "force thickening" is seen, where the effective friction coefficient increases again with increasing force after first having decreased in the vicinity of the delocalization threshold.

6 Summary and outlook

We have presented recent results of a theory for active microrheology in high-density colloidal suspensions, based on the integration through transients formalism (ITT) and mode-coupling theory of the glass transition (MCT). The theory predicts a delocalization threshold for the localized probe-particle motion in the ideal glass. At forces stronger than those corresponding to the rigidity of nearest-neighbor cages, the glass locally shows force-induced melting, allowing for probe motion not only in the direction of the applied force, but also perpendicular to it. This force-induced diffusion is qualitatively understood based on a schematic simplification of MCT.

Recent MD simulations [27,28] have also investigated the mean-squared displacement of the probe particle along the direction of the force, after subtracting the average displacement. This quantity shows faster-than-diffusive growth as a function of time. This has been rationalized based on a trap model with a random distribution of forces. The corresponding schematic-MCT analysis does not recover such superdiffusive behavior [45]. The microscopic ITT-MCT, on the other hand, incorporates subtle effects coupling density fluctuations with different alignment to the applied force, resulting in two different competing large-wavelength asymptotes for the memory kernel in the equations of motion. It has been indicated [42] that this may

be sufficient to recover a transient regime of superdiffusion. Whether superdiffusive motion exists as a true long-time asymptote in the force-direction MSD, remains an open issue.

Another aspect of the probe motion close to the delocalization threshold is its intermittent dynamics, indicated in computer-simulation studies. Within MCT, only averaged quantities are discussed, but it is striking that the probe-particle distribution functions develop heavy tails in the direction of the force, cf. Fig. 4. A careful discussion of these tails and their behavior with increasing force will be fruitful.

One of the issues discussed in the context of microrheology is the connection of its response to the macroscopic rheological properties of the embedding host system [1]. Usually, this is restricted to the linear-response regime. In the nonlinear response regime, the existence of a delocalization threshold indicates a local melting-by-driving of the glass-forming host. Its macroscopic analog is the yielding of amorphous soft solids under macroscopic stress. This has been analyzed in recent experiments on a colloidal hard-sphere-like glass [55]. The macroscopic deformation $\gamma(t)$ under constant applied stress can be rationalized in the spirit of ITT combined with a simple rheological model accounting for shear thinning – the macroscopic analog of the force-thinning behavior seen in Fig. 2. Qualitatively, $\gamma(t)$ displays the same transient behavior as the single-particle displacement $\delta z(t)$ for the microrheological probe driven by a constant force [56]. It will be interesting to establish such a connection based on a fully microscopic theory of glassy dynamics.

The work discussed here has been performed in project A7 of the SFB-Transregio TR6 “The Physics of Colloidal Dispersions in External Fields”, funded by the Deutsche Forschungsgemeinschaft (DFG) in 2010–2013. We thank I. Gazuz, M.V. Gnann, and Ch.J. Harrer for joint work on this project. We also thank A.M. Puertas for the fruitful cooperation and discussions, and D. Winter and J. Horbach (project A5) for collaboration. Th.V. also acknowledges funding from the Helmholtz-Gemeinschaft (HGF) and the Zukunftskolleg der Universität Konstanz.

References

1. T.A. Waigh, Rep. Prog. Phys. **68**, 685 (2005)
2. P. Cicuta, A.M. Donald, Soft Matter **3**, 1449 (2007)
3. Y. Kimura, J. Phys. Soc. Jpn. **78**, 041005 (2009)
4. T.M. Squires, T.G. Mason, Annu. Rev. Fluid Mech. **42**, 413 (2010)
5. A. Erbe, M. Zientara, L. Baraban, C. Kreidler, P. Leiderer, J. Phys.: Condens. Matter **20**, 404215 (2008)
6. C. Gutsche, F. Kremer, M. Krüger, M. Rauscher, R. Weeber, J. Harting, J. Chem. Phys. **129**, 084902 (2008)
7. A.S. Khair, T.M. Squires, Phys. Rev. Lett. **105**, 156001 (2010)
8. J.S. Lintuvuori, K. Stratford, M.E. Cates, D. Marenduzzo, Phys. Rev. Lett. **105**, 178302 (2010)
9. J.P. Rich, J. Lammerding, G.H. McKinley, P.S. Doyle, Soft Matter **7**, 9933 (2011)
10. R. Candelier O. Dauchot, Phys. Rev. Lett. **103**, 128001 (2009)
11. Y. Ding, N. Gravish, D.I. Goldman, Phys. Rev. Lett. **106**, 028001 (2011)
12. A. Seguin, Y. Bertho, P. Gondret, J. Crassous, Phys. Rev. Lett. **107**, 048001 (2011)
13. A. Fiege, M. Grob, A. Zippelius, Granular Matter **14**, 247 (2012)
14. A.W.C. Lau, B.D. Hoffman, A. Davies, J.C. Crocker, T.C. Lubensky, Phys. Rev. Lett. **91**, 198101 (2003)
15. C. Wilhelm, Phys. Rev. Lett. **101**, 028101 (2008)
16. D. Robert, K. Aubertin, J.-C. Bacri, C. Wilhelm, Phys. Rev. E **85**, 011905 (2012)
17. D. Wirtz, Anuu. Rev. Biophys. **38**, 301 (2009)

18. M.B. Hastings, C.J. Olson Reichhardt, C. Reichhardt, Phys. Rev. Lett. **90**, 098302 (2003)
19. P. Habdas, D. Schaar, A.C. Levitt, E.R. Weeks, Europhys. Lett. **67**, 477 (2004)
20. S.R. Williams, D.J. Evans, Phys. Rev. Lett. **96**, 015701 (2006)
21. T.M. Squires, Langmuir **24**, 1147 (2008)
22. R.N. Zia, J.F. Brady, J. Fluid Mech. **658**, 188 (2010)
23. R.N. Zia, J.F. Brady, J. Rheol. (NY) **56**, 1175 (2012)
24. R.J. DePuit, T.M. Squires, J. Phys.: Condens. Matter **24**, 464106 (2012)
25. R.J. DePuit, T.M. Squires, J. Phys.: Condens. Matter **24**, 464107 (2012)
26. R.L. Jack, D. Kelsey, J. Garrahan, D. Chandler, Phys. Rev. E **78**, 011506 (2008)
27. D. Winter, J. Horbach, P. Virnau, K. Binder, Phys. Rev. Lett. **108**, 028303 (2012)
28. D. Winter, J. Horbach, J. Chem. Phys. **138**, 12A512 (2013)
29. I. Sriram, E.M. Furst, R.J. DePuit, T.M. Squires, J. Rheol. **53**, 357 (2009)
30. I. Sriram, A. Meyer, E.M. Furst, Phys. Fluids **22**, 062003 (2010)
31. L.G. Wilson, A.W. Harrison, W.C.K. Poon, A.M. Puertas, Europhys. Lett. **93**, 58007 (2011)
32. E.M. Furst, Curr. Opin. Colloid Interface Sci. **10**, 79 (2005)
33. L.G. Wilson, A.W. Harrison, A.B. Schofield, J. Arlt, W.C.K. Poon, J. Phys. Chem. B **113**, 3806 (2009)
34. W. Götze, Complex Dynamics of Glass-Forming Liquids (Oxford University Press, 2009)
35. K. Kawasaki, J.D. Gunton, Phys. Rev. A **8**, 2048 (1973)
36. D.J. Evans, G. Morriss, Statistical Mechanics of Nonequilibrium Liquids (Cambridge University Press, 2008)
37. M. Fuchs, M.E. Cates, Phys. Rev. Lett. **89**, 248304 (2002)
38. M. Fuchs, M.E. Cates, J. Rheol. (NY) **53**, 957 (2009)
39. I. Gazuz, A.M. Puertas, Th. Voigtmann, M. Fuchs, Phys. Rev. Lett. **102**, 248302 (2009)
40. I. Gazuz, M. Fuchs, Phys. Rev. E **87**, 032304 (2013)
41. Ch.J. Harrer, A.M. Puertas, Th. Voigtmann, M. Z. Phys. Chem. **226**, 779 (2012)
42. Ch.J. Harrer, *Active and Nonlinear Microrheology of Dense Colloidal Suspensions*, P.h.D thesis, Universität Konstanz, 2013
43. J.M. Brader, Th. Voigtmann, M. Fuchs, R.G. Larson, M.E. Cates, Proc. Natl. Acad. Sci. USA **106**, 15186 (2009)
44. M.V. Gnann, I. Gazuz, A.M. Puertas, M. Fuchs, Th. Voigtmann, Soft Matter **7**, 1390 (2011)
45. Ch.J. Harrer, D. Winter, J. Horbach, M. Fuchs, Th. Voigtmann, J. Phys.: Condens. Matter **24**, 464105 (2012)
46. M.V. Gnann, Th. Voigtmann, Phys. Rev. E **86**, 011406 (2012)
47. I.C. Carpen, J.F. Brady, J. Rheol. **49**, 1483 (2005)
48. Th. Voigtmann, EPL **96**, 36006 (2011)
49. B. Cichocki, W. Hess, Physica A **141**, 475 (1987)
50. K. Kawasaki, Physica A **215**, 61 (1995)
51. W. Hess, R. Klein, Adv. Phys. **32**, 173 (1983)
52. J.-P. Hansen, I.R. McDonald, *Theory of Simple Liquids*, 2nd edn. (Academic Press Limited, London, 1986)
53. T.M. Squires, J.F. Brady, Phys. Fluids **17**, 073101 (2005)
54. A.M. Puertas, AIP Conf. Proc. **1319**, 141 (2010)
55. M. Siebenbürger, M. Ballauff, Th. Voigtmann, Phys. Rev. Lett. **108**, 255701 (2012)
56. Th. Voigtmann, Slow Dynamics in External Forces: Creep and Microrheology, in *4th International Symposium on Slow Dynamics in Complex Systems*, edited by M. Tokuyama, I. Oppenheim, Vol. 1518 of AIP Conf. Proc. (AIP, 2013), p. 94